

This is the accepted manuscript made available via CHORUS. The article has been published as:

# Lattice vacancies responsible for the linear dependence of the low-temperature heat capacity of insulating materials

Jacob M. Schliesser and Brian F. Woodfield

Phys. Rev. B **91**, 024109 — Published 29 January 2015

DOI: [10.1103/PhysRevB.91.024109](https://doi.org/10.1103/PhysRevB.91.024109)

# Lattice vacancies responsible for the linear dependence on the low temperature heat capacity of insulating materials

Jacob M. Schliesser and Brian F. Woodfield\*

*Department of Chemistry and Biochemistry, Brigham Young University, Provo, UT 84602*

\*Corresponding author. Tel.: +1 801 422 2093; fax: +1 801 422 0153.

*E-mail address:* [brian\\_woodfield@byu.edu](mailto:brian_woodfield@byu.edu) (B. F. Woodfield)

## Abstract

The linear dependence on temperature ( $\gamma T$ ) of the heat capacity at low temperatures ( $T < 15$  K) is traditionally attributed to conduction electrons in metals; however, many insulators also exhibit a linear dependence that has been attributed to a variety of other physical properties. The property most commonly used to justify the presence of this linear dependence is lattice vacancies, but a correlation between these two properties has never been shown. We have devised a theory that justifies a linear heat capacity as a result of lattice vacancies, and we provide measured values and data from the literature to support our arguments. We postulate that many small Schottky anomalies are produced by a puckering of the lattice around these vacancies, and variations in the lattice caused by position or proximity to some form of structure result in a distribution of Schottky anomalies with different energies. We present a mathematical model to describe these anomalies and their distribution based on literature data that ultimately results in a linear heat capacity. From these calculations, a quantitative relationship between the linear term and the concentration of lattice vacancies is identified, and we verify these calculations using values of  $\gamma$  and vacancy concentrations for several materials. We have compiled many values of  $\gamma$  and vacancy concentrations from the literature which show several significant trends that provide further evidence for our theory.

**Keywords:** heat capacity, low temperature, linear term, lattice vacancies, Schottky defects, insulators

## I. INTRODUCTION

### A. Linear Heat Capacity at Low Temperatures

Traditionally, the linear dependence on temperature of the low temperature ( $T < 15$  K) heat capacity has been associated with conduction electrons in metals [1, 2], but a linear term,  $\gamma T$ , has been found in many non-metallic materials as well [3-5]. The linear dependence of these materials has been an area of great interest and has resulted in a number of theories having broad and often inconsistent origins.

In metals, the linear dependence arises from electrons that populate energy levels above the Fermi level at any finite temperature [1, 2]. High temperature ceramic superconductors have been found to show a linear dependence in the heat capacity. This could easily be misinterpreted as arising from conduction electrons similar to those in metals, but because the conductivity arises from Cooper pairs [6], which behave as bosons rather than fermions, new theories were needed to explain the linear dependence.

Many theories suggested the linear dependence was intrinsic to superconductivity [4, 7-10], while others have attributed the linear term to a tunneling-system related to oxygen [11], impurity phases such as  $\text{BaCuO}_2$  in  $\text{YBa}_2\text{Cu}_3\text{O}_7$  (YBCO) [12], or twin boundaries and oxygen vacancies [13-15]. The arguments of those against an intrinsic linear term are that linear terms are inconsistent from sample to sample and depend strongly on sample quality [4, 10]; furthermore, some superconductors that become insulators at certain stiochiometries retain a similar linear term in the heat capacity even as insulators [16, 17].

Several studies have attempted to identify the origins of the linear terms in insulating materials resulting in theories as diverse as the samples. Table I lists the linear terms of several insulating materials as determined from a combination of adiabatic [18-25], semi-adiabatic pulse

[19-23, 26-30], isothermal [21, 26], and relaxation calorimetry methods [5, 18, 21, 27, 31-43], and Fig. 1 graphically shows a sampling of these linear terms relative to each other. The linear term in  $\text{BaCuO}_2$  has been attributed to magnetic degrees of freedom [23] but has also been disregarded simply because it is an insulator [44]. Nanocrystalline magnetite ( $\text{Fe}_3\text{O}_4$ ) and hematite ( $\text{Fe}_2\text{O}_3$ ) have linear terms that have been attributed to superparamagnetism [19, 31]. The linear terms in several vanadium bronzes have been attributed to singlet bipolarons [24]. In several insulating layered oxides, the linear terms are attributed to a localized density of states associated with lattice vacancies [5]. Many investigations of insulators with linear terms adopt some form of this latter explanation since lattice vacancies are inherent to all materials to some degree; however, the only derivation of a linear heat capacity from lattice vacancies treats the vacancies the same as a free-electron gas where vacancies “move practically freely through a crystal”, which is wholly unsupported in the original manuscript [45].

In glasses, the linear dependence on the low temperature heat capacity has been attributed to particles trapped in defect sites that create a particle-in-a-box system [46, 47], but a more common theory is based on a system of tunneling states [3, 48, 49]. This theory assumes that there are two equilibrium orientations that atoms or groups of atoms can have. The two energy minima associated with each of these orientations are separated by an energy barrier that must be overcome by phonon-assisted tunneling in order for the atoms to shift from one orientation to the other. The separation in energy between the two minima is different for every group of atoms because of local strains and the local configuration of the atoms around the group. Each of these two-level systems (TLS) for which the tunneling barrier is not too large results in a Schottky anomaly in the low temperature heat capacity [1]

$$C_{Sch} = n_{Sch}(\theta)k \left(\frac{\theta}{T}\right)^2 \frac{e^{\theta/T}}{(1 + e^{\theta/T})^2} \quad (1)$$

where  $\theta$  is the energy separation of the two states with units of K ( $\theta = \Delta E/k$ ),  $n_{Sch}(\theta)$  is the moles of anomalies per mole of material for a given separation  $\theta$ , and  $k$  is the Boltzmann constant.

Because the number and energies of these tunneling systems is random, the distribution  $n_{Sch}(\theta)$  can be assumed to be a constant value  $n(0)$ , which makes the sum of all Schottky anomalies approximated by the integral [3]

$$C_{lin}(T) = \int_0^\infty n_{Sch}(\theta)k \left(\frac{\theta}{T}\right)^2 \frac{e^{\theta/T}}{(1 + e^{\theta/T})^2} d\theta \approx \frac{\pi^2}{6} k^2 n(0) T \quad (2)$$

where  $n(0)$  is the number of contributing TLSs per mole of sample per unit energy. As seen in eqn. 2 the heat capacity contribution from these TLSs is linear with temperature.

The original manuscript by Anderson, Halperin, and Varma outlining this theory provides no support for the use of a TLS believed to produce a Schottky anomaly or justification for a random distribution of energies produced by the TLSs. Several others have recognized this and have attempted to provide evidence for these properties while others have modified the model to make the TLS and distribution more meaningful [11, 24, 50, 51]. A major flaw in this theory is this lack of understanding the source and distribution of the TLSs.

To understand the distribution one must first understand the heat capacity that is produced by it. The linear heat capacity in metals exists up to high temperatures (O(1000 K)) but is generally undetectable due to the much larger contribution from phonons at temperatures any higher than about 15 K; however, the linear term in insulating materials does not extend up to high temperatures, and the extent to which the linear term is nonzero/non-negligible has been investigated by several groups. Anderson *et al* claimed that the linear term of glasses must exist

up to about 10 K before vanishing [3]. Investigations of BaCuO<sub>2</sub> have shown that this contribution to the heat capacity remains linear until about 30 K where it begins to decrease until becoming negligible around 40 to 50 K [23, 44]. Others investigating the heat capacity of Fe<sub>2</sub>P<sub>2</sub>O<sub>7</sub> claim that the linear term begins to decrease between 15 – 20 K [34]. McWhan's study of several doped Al<sub>2</sub>O<sub>3</sub> compounds shows linearity until about 25 K above which the slope ( $\gamma$ ) quickly decreases to zero [51]. Data of TiO<sub>2</sub> from Sandin show an excess heat capacity that increases approximately linearly until about 15 K then quickly drops to zero by about 20 K [52]. Therefore, we will consider the shape of this excess heat capacity to be linear up to about 15 K at which point, it decreases until becoming negligible around 50 K.

The broad range of insulating materials that have a linear heat capacity and the relatively similar cutoff temperature of these linear terms suggests that there exists a common underlying factor in all of these materials that produces the linear dependence in the low temperature heat capacity.

### **B. Lattice Vacancies**

Lattice vacancies appear in all materials to some degree. At thermal equilibrium the concentration of vacancies can be estimated using the Boltzmann factor (for  $n_{vac} \ll N$ ) [2]:

$$n_{vac}/N \cong \exp(-E_v/kT) \quad (3)$$

where  $n_{vac}/N$  is the ratio of the number of lattice vacancies  $n_{vac}$  to the number of atoms  $N$ ,  $E_v$  is the energy required to remove an atom from the lattice site inside the crystal and place it on the surface,  $k$  is Boltzmann's constant, and  $T$  is the temperature of the crystal or the temperature at which the crystal was calcined if it was suddenly cooled (thereby freezing in vacancies). For a typical  $E_v$  (about 1 eV) and calcination temperature (about 1000 K), eqn. 3 yields a concentration of lattice vacancies on the order of  $10^{-5}$  moles of vacancies per mole of atoms.

Lattice vacancies are generally determined using redox titrations or thermogravimetric analysis (TGA) [53-59], but for nanomaterials and materials with very few vacancies, less conventional methods are required such as EXAFS [60, 61], XANES [61], other X-ray techniques [53, 61], Raman spectroscopy [60, 61], high resolution TEM [61], EELS [62], XEDS [63], STEM [64], neutron diffraction [53, 59], and a plethora of esoteric techniques [65-73]. Each of these methods is limited by experimental error, resolution, or applicability that constrain what samples can be tested and the amount of useful information that can be obtained (hence the large number of specialized techniques). The detection limit for most of these techniques is around parts per thousand or  $n_{vac}/N \approx 10^{-3}$ , making these techniques only suitable for highly nonstoichiometric samples. Table II lists lattice vacancy concentrations of a wide range of materials as measured from these techniques [57-62, 64-74].

When a lattice vacancy is present in a crystal, the atomic structure around the vacancy takes on one of two possible conformations: dimer or puckered [74-77]. Each of these conformations has an energy minimum separated by an energy barrier. These two energy levels would result in a Schottky anomaly in the low temperature heat capacity (eqn. 1) with an energy separation  $\theta$  equal to the difference between the two levels. Surface configurations, which are somewhat similar to vacancies due to their similar coordinations and strain, have been shown to have similar two-level systems that produce Schottky anomalies [78-81].

The energies of the dimer and puckered configurations of amorphous SiO<sub>2</sub> have been investigated by Boero *et al* using first principles calculations approximating the two levels to be separated by an energy difference of about 0.25 eV [75]. Skuja reviewed several articles on spectroscopic methods used to investigate energies associated with vacancies and showed that a spectrum of energy levels up to 0.1 eV arises from vacancies in a typical solid [82]. Rigid unit



modes of  $\text{SiO}_4$  tetrahedra have two-level systems similar to lattice vacancies and have a range of possible energies up to around 500 GHz or about 2 meV [83]. Di Valentin *et al* investigated tunneling related to rotations of surface atoms and found tunneling barriers between about 10 and 20 meV [79]. Gryaznov *et al* discovered lattice vacancy energy levels with energies around 20 meV different from the lattice [84]. Smith investigated librational frequencies covering the range of 30 peV to 33.5 meV [80]. Strong librational frequencies around oxygen vacancies in perovskites have been found to have energies of about  $90 - 120 \text{ cm}^{-1}$  (11 – 15 meV), and a broad spectrum of peaks below  $90 \text{ cm}^{-1}$  have been attributed to thermally induced disorder, which essentially consists of lattice vacancies as eqn. 3 shows [85]. From all these investigations, we conclude that energies associated with lattice vacancies have a broad distribution of possible states, likely caused by differences in the lattice surrounding each vacancy, and have an average maximum of about 20 meV.

From the information presented above, it can be seen that a single lattice vacancy results in a two-level system that is capable of producing a Schottky anomaly in the low temperature heat capacity. Multiple vacancies have a random distribution of energy differences that would yield a distribution of Schottky anomalies. The cutoff of the energies from the TLSs would also produce a cutoff (albeit gradual) in the sum of the Schottky anomalies produced from the vacancies. We will show how the energies associated with TLSs are responsible for the linear term and its cutoff temperature and matches what has been observed experimentally.

## II. THEORY and CORRELATIONS

### A. Distributions

We first consider the distribution of energies associated with the TLSs from vacancies that determine  $n_{Sch}(\theta)$  in eqn. 2. The distribution  $n_{Sch}(\theta)$  used for eqn. 2 assumes that  $n_{Sch}$  is a

single value for all values of  $\theta$  up to infinity, but we will examine several other possible and more meaningful distributions that correspond to the experimental data outlined above and that could produce a linear (or pseudo-linear) heat capacity with an appropriate ending temperature. All of the following distributions have been tailored so that  $n_{Sch}(\theta)$  is negligible by about 150 K (or 13 meV). These distributions use  $\theta$  with units of K rather than meV to be applicable to the Schottky heat capacity as given in eqn. 1. We note here that 1 meV = 11.6 K.

Figure 2 shows several hypothetical distributions of  $n_{Sch}(\theta)$ . A simple Gaussian distribution with  $\theta_{max}$  centered at 30 K and a standard deviation of 40 K is shown in Fig. 2(a). In this distribution,  $n_{Sch}$  at  $\theta = 30$  K corresponds to the average energy produced by vacancies that is more probable than the others perhaps due to the homogeneous nature inside the bulk of the material. The other energies arise because of the vacancies' proximity to grain boundaries, other vacancies, or the surface, which are generally less common than a homogeneous environment. This type of distribution might be suitable for large grain, crystalline materials.

A left skewed Gaussian that has an average  $\theta = 85$  K is shown in Fig. 2(b). The average here would again represent the vacancies in a homogeneous environment likely within the bulk of the material, but the skew would arise from a large concentration of vacancies near some similar inhomogeneous structure such as the surface. This distribution would likely apply to nanomaterials with a high surface to bulk ratio or materials with a high degree of disorder such as amorphous solids.

Figure 2(c) shows the sum of two Gaussian distributions that are centered at 5 K and 75 K with standard deviations of 28 K. These Gaussians would be similar to the one discussed for Fig. 2(a), but here we suppose the low energy Gaussian arises from vacancies near or on the surface where there is less strain, and the high energy Gaussian arises from the vacancies in the

bulk of the material. This distribution may be more meaningful than the others because the center position, height, and width of each Gaussian can be varied as long as the sum has the same general shape. This allows for a different distribution for every sample that has a linear heat capacity and could therefore apply to any type of material.

A step distribution with a cutoff of  $\theta = 150$  K (based on the experimental data outlined above) is shown in Fig. 2(d). This distribution is very similar to the constant value distribution used in eqn. 2 and assumes that the energies associated with the lattice vacancies are completely random and only exist below a particular energy, treating vacancies on the surface, in the bulk, and near defects or grain boundaries the same. The only variable factor in this distribution is the cutoff energy, which Anderson *et al* postulated to be related to the glass transition temperature on the order of 1000 K. Although this distribution simplifies calculations, it is unlikely that vacancies' energies will be completely random because bulk and surface energetics are so different [86], and a meaningful distribution must not ignore surface energies since many of the materials with linear terms are nanoparticles (see Table I).

### **B. Resultant Heat Capacity**

When these distributions are used in eqn. 2, the resultant heat capacity as determined by numerical integration is approximately linear up to about 15 K and then gradually drops towards zero. Figure 3 shows the heat capacity curves (as  $C/T$  versus  $T$  in which a linear heat capacity will appear as a constant) that result from the distributions of Fig. 2. The Gaussian distribution yields a heat capacity that deviates the most from linearity (up to about 15 %) as can be seen in Fig. 3(a). The heat capacity derived from the skewed Gaussian distribution, seen in Fig. 3(b), results in a heat capacity with less than a 5 % deviation from linearity below 15 K. The distribution created by summing two Gaussian results in a heat capacity that deviates from

linearity by less than 0.8 % (see Fig. 3(c)), and the step distribution results in a heat capacity that deviates from linearity by about 0.05 % below 10 K but increases to 0.3 % by 15 K (see Fig. 3(d)). For temperatures much less than the cutoff temperature, the step distribution produces the same linear heat capacity result of eqn. 2. All of these distributions resemble the energies typically produced from lattice vacancies and result in a heat capacity function that resembles what has been observed in many insulating materials, but the sum of two Gaussian distributions appears to be the most meaningful and has a high degree of linearity.

The distributions discussed above are just a few of the possible distributions that result in a linear heat capacity similar to what has been reported in the literature [3, 23, 34, 44, 51, 52]. The actual distributions likely vary from the distributions presented here, but these distributions demonstrate the general shape that  $n_{Sch}(\theta)$  must have. Low temperature heat capacity data can have an uncertainty of about 2 %, and fits can have an uncertainty on the order of 1 %; therefore, the nonlinearity of these derived heat capacities would likely be buried in the error of the data or fit. These results show that lattice vacancies do indeed produce a linear (or pseudo-linear) contribution to the low temperature heat capacity.

### C. Quantification of Vacancies from $\gamma$

Because each Schottky anomaly is a result of a lattice vacancy, the sum of all Schottky anomalies will give a measure of the total number of vacancies  $n_{vac}$  in a given sample. Finding  $n_{vac}$  is simply done by integrating the distribution  $n_{Sch}(\theta)$  over all  $\theta$ . The height or normalization of the distribution will be manifest in the slope or linear term  $\gamma$  of the resultant heat capacity. We have calculated linear terms from typical vacancy concentrations of  $n_{vac} = 10^{-5}$  to 1 vacancies per formula unit (see Table II). Each distribution (see Fig. 2) was normalized to these values, and the linear term was determined by averaging the resultant heat capacity divided by temperature

( $C/T$ ) from 0.5-15 K. These values were then used to determine constants of proportionality for each distribution by fitting to a line with zero intercept. The proportionalities are in the form  $\gamma_{calc} = c \times n_{vac}$ , and values of  $c$  were found to be 157, 151, 115, and 91  $\text{mJ}\cdot\text{mol}^{-1}\cdot\text{K}^{-2}$  for the Gaussian, skewed Gaussian, two-Gaussian, and step distributions, respectively. These calculations have an estimated uncertainty of about 6 % based on the heat capacity data, the fit, and the distribution's linearity, but with better data and fits an uncertainty of about 2% would be reasonable.

#### **D. Comparison to Experimental Data**

To test the results of this model against actual data, we have measured the linear terms and vacancy concentrations of  $\text{Co}_3\text{O}_4$ ,  $\text{Co}_3\text{O}_4$  (n),  $\text{CoO}$  (n),  $\text{Fe}_3\text{O}_4$  (n),  $\text{CuO}$  (n), and  $\text{Al}_2\text{O}_3$  (n) which are part of separate, ongoing projects in our laboratory. The samples were found to have no chemical or phase impurities, and all characterization and thermodynamic data will be reported elsewhere.

The low temperature heat capacities of  $\text{Fe}_3\text{O}_4$  (n),  $\text{CoO}$  (n), and  $\text{Al}_2\text{O}_3$  (n) and the experimental details have been published previously [19, 20, 41]. The other samples' heat capacities were measured on a Quantum Design Physical Properties Measurement System (PPMS) from 1.8 – 300 K following the method of Shi *et al* [87]. Approximately 30 mg of each sample were mixed with copper stips (Alpha Aesar mass fraction purity 0.9995) to provide better thermal contact and put into copper cups that were pressed into pellets. Addenda measurements were performed that measured the heat capacity of the calorimeter and the grease used to attach the sample. After each addenda measurement, the sample was attached to the PPMS puck, and the heat capacity was measured. The system automatically corrects for the heat capacities of the calorimeter and grease, and the heat capacity of the copper was corrected for using data from Stevens and Boerio-Goates [88]. Data measured on the PPMS using this method have an

estimated uncertainty of  $\pm 0.02 \cdot C_p^\circ$  for  $2 < T/K < 10$  and  $\pm 0.01 \cdot C_p^\circ$  for  $10 < T/K < 300$  [87]. The data below 10 K were fit to a theoretical function of the form

$$C(T) = \sum_{i=3,5,7} B_i T^i + \gamma T \quad (4)$$

where the summation term represents the contribution from lattice vibrations, and the linear term is related to lattice vacancies. The fits having the same number of lattice terms but no linear contribution resulted in %RMS values of 7.16, 18.1, and 13.2 for  $\text{Co}_3\text{O}_4$ ,  $\text{Co}_3\text{O}_4$  (n), and  $\text{CuO}$  (n), respectively, whereas the fits including the linear term resulted in %RMS values of 0.82, 1.80, and 1.18. The values of  $\gamma$  obtained from the fits were 2.138, 14.111, and 0.489  $\text{mJ} \cdot \text{mol}^{-1} \cdot \text{K}^{-2}$  for  $\text{Co}_3\text{O}_4$ ,  $\text{Co}_3\text{O}_4$  (n), and  $\text{CuO}$  (n), respectively (see Table I), and the approximated uncertainty in these values is 2.5 % based on the heat capacity data and the fitting error.

The vacancy concentrations of  $\text{Co}_3\text{O}_4$ ,  $\text{Co}_3\text{O}_4$  (n),  $\text{CoO}$  (n), and  $\text{Fe}_3\text{O}_4$  (n) were measured using a thermogravimetric reduction technique. Approximately 20 mg of each sample were placed in Pt crucibles which were inserted into a Mettler Toledo TGA/DSC 1 equipped with an automated GC 200 gas controller. To remove any surface-bound water the samples were heated to 400 °C in He and cooled back to room temperature. The reduction gas was 10 %  $\text{H}_2$  in He with a flow rate of  $100 \text{ mL} \cdot \text{min}^{-1}$ , and the samples were heated at a rate of  $3 \text{ }^\circ\text{C} \cdot \text{min}^{-1}$  to 900 °C. Reduction occurred abruptly at about 300 °C for the cobalt oxides and at about 400 for the iron oxide and resulted in mass losses of 26.5310 %, 25.9726 %, 18.50 %, and 28.50 % corresponding to stoichiometries of  $\text{Co}_3\text{O}_{3.9905}$ ,  $\text{Co}_3\text{O}_{3.8770}$  (n),  $\text{CoO}_{0.8361}$  (n), and  $\text{Fe}_{2.8750}\text{O}_4$  (n) respectively, yielding vacancy concentrations of  $n_{vac} = 0.0095$ , 0.1230, 0.1639, and 0.1250. The approximated uncertainty of these values is 15 %.

The vacancy concentration of  $\text{CuO}$  (n) was determined by performing Rietveld refinement on powder X-ray diffraction (XRD) data collected at 100 K.  $\text{CuO}$  powder was packed

into a polyimide capillary with an inner diameter of 0.012 mm, and XRD data were collected in transmission mode using a MACH3 four circle single crystal diffractometer coupled to a Bruker Apex II CCD detector with a Bruker-Nonius FR591 rotating anode X-ray source producing Cu  $K_\alpha$  radiation ( $\lambda = 1.5418 \text{ \AA}$ ). Data were collected between  $2^\circ - 133^\circ 2\theta$  by performing a series of 8 overlapping phi 360 scans. The Bruker XRD<sup>2</sup> program was used to merge the images and integrate the intensity of the diffraction rings. Rietveld refinement was performed using the PANalytical Highscore Plus software. The details of the analysis will be published elsewhere, but from the refinement, copper atoms were found to be slightly deficient yielding  $\text{Cu}_{0.9891}\text{O}$  or  $n_{vac} = 0.0109$  having an approximate uncertainty of 10 %.

The vacancy concentration of  $\text{Al}_2\text{O}_3$  (n) was determined using eqn. 3 and the value of  $E_v$  (0.18 eV) from ref. [89]. Although the  $\text{Al}_2\text{O}_3$  (n) samples used to determine  $\gamma$  were calcined at 973 K, we can assume that  $T \approx 300 \text{ K}$  because the samples were cooled slowly to room temperature after calcination but were cooled quickly from room temperature to perform heat capacity measurements [41]. Using these values in eqn. 3 and accounting for the five atoms per formula unit gives an  $n_{vac}$  of 0.0047 moles of vacancies per mole of  $\text{Al}_2\text{O}_3$  (n). The estimated uncertainty of  $n_{vac}$  determined using this method is 50 %.

All these values of  $\gamma$  and  $n_{vac}$  are plotted in Fig. 4 along with the proportionalities derived herein. The plot shows how  $\gamma$  increases as  $n_{vac}$  increases. The error bars represent the uncertainties discussed above for each value of  $n_{vac}$ , and the uncertainty in  $\gamma$  of 2.5 % is smaller than the size of the symbols. The deviations of the ratio of the actual values of  $\gamma$  and  $n_{vac}$  ( $c = \gamma/n_{vac}$ ) from our calculations are 40 % (using the Gaussian distribution) for  $\text{Al}_2\text{O}_3$ , 30 % (using the Gaussian distribution) for  $\text{Co}_3\text{O}_4$ , 100 % (using the step distribution) for  $\text{CuO}$  (n), 6.3 %

(using 2-Gaussian distributions) for  $\text{Co}_3\text{O}_4$  (n), 230 % (using the step distribution) for  $\text{Fe}_3\text{O}_4$  (n), 150 % (using the step distribution) for  $\text{CoO}$  (n).

The experimental values of  $\gamma$  and  $n_{vac}$  differ from our theoretical values by at most a factor of two or three and as little as a few percent. When all the uncertainties are taken into account, these calculations show qualitative agreement as well as quantitative agreement providing further evidence that the linear term of insulating materials does indeed stem from lattice vacancies. As further evidence supporting our claims, we note that the differences between the measured and calculated values of  $\gamma$  from  $n_{vac}$  are similar despite the method used to determine  $n_{vac}$ .

### E. Trends in $\gamma$ and $n_{vac}$

As a final note, we recognize several trends emphasizing our conclusions. All values of  $\gamma$  found in Table I lie between  $0.01 \text{ mJ}\cdot\text{mol}^{-1}\cdot\text{K}^{-2}$  and  $100 \text{ mJ}\cdot\text{mol}^{-1}\cdot\text{K}^{-2}$ , and values of  $n_{vac}$  in Table II lie between  $10^{-5}$  and 1, which is the same range of values we would expect when applying our calculations to  $\gamma$ . Values of  $\gamma$  for nano phase  $\text{TiO}_2$ ,  $\text{CoO}$ ,  $\text{Co}_3\text{O}_4$ ,  $\alpha\text{-Fe}_2\text{O}_3$ ,  $\text{CuO}$ ,  $\text{SnO}_2$ , and  $\text{ZnO}$  are all larger than the bulk phase values of  $\gamma$ . Values of  $n_{vac}$  from Table II also increase as particle size decreases for  $\text{CeO}_2$  and  $\text{Fe}_3\text{O}_4$ . The Co doped  $\text{ZnO}$  and Al doped  $\text{TiO}_2$  systems have  $\gamma$  much greater than what would be expected for a simple  $\text{CoO}/\text{ZnO}$  or  $\text{Al}_2\text{O}_3/\text{TiO}_2$  mixture, and values of  $n_{vac}$  for  $\text{TiO}_2$  are also larger when dopants are present. Mitchell has also shown that the concentration of defects increases with increasing dopant concentrations [72].

## III. CONCLUSION

We have shown that the linear term, which is often necessary to fit the low temperature heat capacity data for nonmetallic materials, is related to the number of lattice vacancies. We have created several distributions of  $n_{Sch}(\theta)$  that have similar energy cutoffs to experimental data



from the literature and are physically meaningful. The vacancy energies associated with these distributions are assumed to result in small Schottky anomalies due to a puckering of the lattice. These distributions have been shown to produce a linear heat capacity similar to what has been observed for these kinds of materials. We have measured values of  $\gamma$  and  $n_{vac}$  of several samples and compared those to our theoretical values. These values show qualitative and quantitative agreement with our model, and linear terms and lattice vacancy concentrations have been shown to have many similar trends providing further evidence for our arguments. This manuscript provides meaningful evidence supporting the claim that the linear term in insulating materials results from lattice vacancies.

#### **ACKNOWLEDGEMENTS**

We would like to thank Kamyar Keyvanloo and McCallin Fisher for help with the TGA experiments and Dr. Stacey Smith for help with the XRD experiment. This work was financially supported by a grant from the U.S. Department of Energy under grant DE-FG02-05ER15666.

## References

- [1] E. S. R. Gopal, *Specific heats at low temperatures* (Plenum Press New York, 1966), Vol. 227.
- [2] C. Kittel and P. McEuen, *Introduction to solid state physics* (Wiley New York, 1996), Vol. 7.
- [3] P. W. Anderson, B. Halperin, and C. M. Varma, *Philosophical Magazine* **25**, 1 (1972).
- [4] N. E. Phillips, J. P. Emerson, R. A. Fisher, J. E. Gordon, B. F. Woodfield, and D. A. Wright, *Physica C: Superconductivity* **235–240, Part 3**, 1737 (1994).
- [5] J. M. D. Coey, S. Von Molnar, and A. Torressen, *Journal of the Less Common Metals* **151**, 191 (1989).
- [6] J. Bardeen, L. N. Cooper, and J. R. Schrieffer, *Physical Review* **108**, 1175 (1957).
- [7] R. Fisher, J. Gordon, and N. Phillips, *Journal of Superconductivity* **1**, 231 (1988).
- [8] N. E. Phillips, R. Fisher, J. Gordon, S. Kim, A. Stacy, M. Crawford, and E. McCarron III, *Physical review letters* **65**, 357 (1990).
- [9] D. Wright, J. Emerson, B. Woodfield, J. Gordon, R. Fisher, and N. Phillips, *Physical review letters* **82**, 1550 (1999).
- [10] N. E. Phillips, J. P. Emerson, R. A. Fisher, J. E. Gordon, B. F. Woodfield, and D. A. Wright, *Journal of Superconductivity* **7**, 251 (1994).
- [11] B. Golding, N. Birge, W. Haemmerle, R. Cava, and E. Rietman, *Physical Review B* **36**, 5606 (1987).
- [12] D. Eckert, A. Junod, A. Bezingue, T. Graf, and J. Muller, *Journal of Low Temperature Physics* **73**, 241 (1988).

- [13] K. A. Moler, D. L. Sisson, J. S. Urbach, M. R. Beasley, A. Kapitulnik, D. J. Baar, R. Liang, and W. N. Hardy, *Physical Review B* **55**, 3954 (1997).
- [14] J. Emerson, D. Wright, B. Woodfield, S. Reklis, J. Gordon, R. Fisher, and N. Phillips, *Journal of Low Temperature Physics* **105**, 897 (1996).
- [15] J. Emerson, D. Wright, B. Woodfield, J. Gordon, R. Fisher, and N. Phillips, *Physical review letters* **82**, 1546 (1999).
- [16] R. McCallum, D. Johnston, C. Luengo, and M. Maple, *Journal of Low Temperature Physics* **25**, 177 (1976).
- [17] K. Kumagai, Y. Nakamichi, I. Watanabe, Y. Nakamura, H. Nakajima, N. Wada, and P. Lederer, *Physical review letters* **60**, 724 (1988).
- [18] A. Junod, D. Eckert, G. Triscone, J. Müller, and W. Reichardt, *Journal of Physics: Condensed Matter* **1**, 8021 (1989).
- [19] C. L. Snow, Q. Shi, J. Boerio-Goates, and B. F. Woodfield, *The Journal of Physical Chemistry C* **114**, 21100 (2010).
- [20] L. Wang, K. Vu, A. Navrotsky, R. Stevens, B. F. Woodfield, and J. Boerio-Goates, *Chemistry of materials* **16**, 5394 (2004).
- [21] J. Lashley, R. Stevens, M. Crawford, J. Boerio-Goates, B. Woodfield, Y. Qiu, J. Lynn, P. Goddard, and R. Fisher, *Physical Review B* **78**, 104406 (2008).
- [22] S. J. Smith, R. Stevens, S. Liu, G. Li, A. Navrotsky, J. Boerio-Goates, and B. F. Woodfield, *American Mineralogist* **94**, 236 (2009).
- [23] R. A. Fisher, D. A. Wright, J. P. Emerson, B. F. Woodfield, N. E. Phillips, Z. R. Wang, and D. C. Johnston, *Physical Review B* **61**, 538 (2000).
- [24] B. Chakraverty, M. Sienko, and J. Bonnerot, *Physical Review B* **17**, 3781 (1978).

- [25] J. M. D. Coey, M. Viret, L. Ranno, and K. Ounadjela, Physical review letters **75**, 3910 (1995).
- [26] J. Majzlan, A. Navrotsky, B. F. Woodfield, B. E. Lang, J. Boerio-Goates, and R. A. Fisher, Journal of Low Temperature Physics **130**, 69 (2003).
- [27] C. L. Snow, S. J. Smith, B. E. Lang, Q. Shi, J. Boerio-Goates, B. F. Woodfield, and A. Navrotsky, The Journal of Chemical Thermodynamics **43**, 190 (2011).
- [28] R. Stephens, Physical Review B **8**, 2896 (1973).
- [29] J. M. Schliesser, S. J. Smith, G. Li, L. Li, T. F. Walker, T. Parry, J. Boerio-Goates, and B. F. Woodfield, The Journal of Chemical Thermodynamics (2014).
- [30] J. M. Schliesser, S. J. Smith, G. Li, L. Li, T. F. Walker, T. Perry, J. Boerio-Goates, and B. F. Woodfield, The Journal of Chemical Thermodynamics (2014).
- [31] C. L. Snow, C. R. Lee, Q. Shi, J. Boerio-Goates, and B. F. Woodfield, The Journal of Chemical Thermodynamics **42**, 1142 (2010).
- [32] C. Snow, K. Lilova, A. Radha, Q. Shi, S. Smith, A. Navrotsky, J. Boerio-Goates, and B. Woodfield, The Journal of Chemical Thermodynamics **58**, 307 (2013).
- [33] C. L. Snow, Q. Shi, J. Boerio-Goates, and B. F. Woodfield, The Journal of Chemical Thermodynamics **42**, 1136 (2010).
- [34] Q. Shi, L. Zhang, M. E. Schlesinger, J. Boerio-Goates, and B. F. Woodfield, The Journal of Chemical Thermodynamics **61**, 51 (2013).
- [35] Q. Shi, L. Zhang, M. E. Schlesinger, J. Boerio-Goates, and B. F. Woodfield, The Journal of Chemical Thermodynamics **62**, 86 (2013).
- [36] Q. Shi, L. Zhang, M. E. Schlesinger, J. Boerio-Goates, and B. F. Woodfield, The Journal of Chemical Thermodynamics **62**, 35 (2013).

- [37] Q. Shi, J. Boerio-Goates, K. Woodfield, M. Rytting, K. Pulsipher, E. C. Spencer, N. L. Ross, A. Navrotsky, and B. F. Woodfield, *The Journal of Physical Chemistry C* **116**, 3910 (2012).
- [38] C. Ma, Q. Shi, B. F. Woodfield, and A. Navrotsky, *The Journal of Chemical Thermodynamics* **60**, 191 (2013).
- [39] W. Zhou, Q. Shi, B. F. Woodfield, and A. Navrotsky, *The Journal of Chemical Thermodynamics* **43**, 970 (2011).
- [40] Q. Shi, T.-J. Park, J. Schliesser, A. Navrotsky, and B. F. Woodfield, *The Journal of Chemical Thermodynamics* **72**, 77 (2014).
- [41] E. C. Spencer, B. Huang, S. F. Parker, A. I. Kolesnikov, N. L. Ross, and B. F. Woodfield, *The Journal of chemical physics* **139**, 244705 (2013).
- [42] R. E. Olsen, T. M. Alam, C. H. Bartholomew, D. B. Enfield, J. Schliesser, and B. F. Woodfield, *The Journal of Physical Chemistry C* **118**, 9176 (2014).
- [43] M. A. Ribeiro da Silva, M. D. Ribeiro da Silva, A. I. Lobo Ferreira, Q. Shi, B. F. Woodfield, and R. N. Goldberg, *The Journal of Chemical Thermodynamics* (2012).
- [44] J.-Y. Genoud, A. Mirmelstein, G. Triscone, A. Junod, and J. Muller, *Physical Review B* **52**, 12833 (1995).
- [45] A. Andreev and I. Lifshits, *ZHUR EKSPER TEORET FIZIKI* **56**, 2057 (1969).
- [46] H. B. Rosenstock, *Journal of Non-Crystalline Solids* **7**, 123 (1972).
- [47] R. A. Fisher, *Journal of Non-Crystalline Solids* **41**, 251 (1980).
- [48] W. Phillips, *Journal of Low Temperature Physics* **7**, 351 (1972).
- [49] W. Phillips, *Reports on Progress in Physics* **50**, 1657 (1987).

- [50] J. Xu, J. Tang, K. Sato, Y. Tanabe, H. Miyasaka, M. Yamashita, S. Heguri, and K. Tanigaki, *Physical Review B* **82**, 085206 (2010).
- [51] D. McWhan, C. Varma, F. Hsu, and J. Remeika, *Physical Review B* **15**, 553 (1977).
- [52] T. Sandin and P. Keesom, *Physical Review* **177**, 1370 (1969).
- [53] Z. L. Wang, J. S. Yin, and Y. D. Jiang, *Micron* **31**, 571 (2000).
- [54] L. Liu, T. Lee, L. Qiu, Y. Yang, and A. Jacobson, *Materials research bulletin* **31**, 29 (1996).
- [55] J. Mizusaki, Y. Mima, S. Yamauchi, K. Fueki, and H. Tagawa, *Journal of solid state chemistry* **80**, 102 (1989).
- [56] M. H. Lankhorst, H. Bouwmeester, and H. Verweij, *Journal of solid state chemistry* **133**, 555 (1997).
- [57] Y. D. Tretyakov, V. Komarov, N. Prosvirina, and I. Kutsenok, *Journal of solid state chemistry* **5**, 157 (1972).
- [58] Y. Matsuda, M. Karppinen, Y. Yamazaki, and H. Yamauchi, *Journal of Solid State Chemistry* **182**, 1713 (2009).
- [59] S. McIntosh, J. F. Vente, W. G. Haije, D. H. A. Blank, and H. J. M. Bouwmeester, *Chemistry of Materials* **18**, 2187 (2006).
- [60] I. Kosacki, T. Suzuki, H. U. Anderson, and P. Colomban, *Solid State Ionics* **149**, 99 (2002).
- [61] Q. Wu, Q. Zheng, and R. van de Krol, *The Journal of Physical Chemistry C* **116**, 7219 (2012).
- [62] Z. L. Wang, J. Yin, Y. Jiang, and J. Zhang, *Applied physics letters* **70**, 3362 (1997).

- [63] T. Mayer, J. Elam, S. George, P. Kotula, and R. Goeke, *Applied Physics Letters* **82**, 2883 (2003).
- [64] Y.-M. Kim *et al.*, *Nature Materials* **11**, 888 (2012).
- [65] C. S. Enache, J. Schoonman, and R. Van Krol, *Journal of electroceramics* **13**, 177 (2004).
- [66] Y. Chiang, E. Lavik, I. Kosacki, H. Tuller, and J. Ying, *Journal of Electroceramics* **1**, 7 (1997).
- [67] M. Janousch, G. I. Meijer, U. Staub, B. Delley, S. F. Karg, and B. P. Andreasson, *Advanced Materials* **19**, 2232 (2007).
- [68] J.-H. Hwang and T. O. Mason, *Zeitschrift für Physikalische Chemie* **207**, 21 (1998).
- [69] K. L. Duncan, Y. Wang, S. R. Bishop, F. Ebrahimi, and E. D. Wachsman, *Journal of the American Ceramic Society* **89**, 3162 (2006).
- [70] F. Schedin, E. Hill, G. Van der Laan, and G. Thornton, *Journal of applied physics* **96**, 1165 (2004).
- [71] M. O'Keeffe and W. J. Moore, *The Journal of Chemical Physics* **36**, 3009 (1962).
- [72] T. E. Mitchell, *Journal of the American Ceramic Society* **82**, 3305 (1999).
- [73] J. Koenitzer, P. Keesom, and J. Honig, *Physical Review B* **39**, 6231 (1989).
- [74] A. S. Mysovsky, P. V. Sushko, S. Mukhopadhyay, A. H. Edwards, and A. L. Shluger, *Physical Review B* **69**, 085202 (2004).
- [75] M. Boero, A. Pasquarello, J. Sarnthein, and R. Car, *Physical review letters* **78**, 887 (1997).
- [76] C. G. Van de Walle and P. Blöchl, *Physical Review B* **47**, 4244 (1993).
- [77] P. E. Blöchl, *Physical Review B* **62**, 6158 (2000).

- [78] J. Boerio-Goates, S. J. Smith, S. Liu, B. E. Lang, G. Li, B. F. Woodfield, and A. Navrotsky, *The Journal of Physical Chemistry C* **117**, 4544 (2013).
- [79] C. Di Valentin, A. Tilocca, A. Selloni, T. Beck, A. Klust, M. Batzill, Y. Losovyj, and U. Diebold, *Journal of the American Chemical Society* **127**, 9895 (2005).
- [80] D. Smith, *Chemical reviews* **94**, 1567 (1994).
- [81] J. C. M. Li and K. S. Pitzer, *The Journal of Physical Chemistry* **60**, 466 (1956).
- [82] L. Skuja, *Journal of Non-Crystalline Solids* **239**, 16 (1998).
- [83] U. Buchenau, N. Nücker, and A. Dianoux, *Physical Review Letters* **53**, 2316 (1984).
- [84] D. Gryaznov, E. Blokhin, A. Sorokine, E. A. Kotomin, R. A. Evarestov, A. Bussmann-Holder, and J. Maier, *The Journal of Physical Chemistry C* **117**, 13776 (2013).
- [85] P. Colomban, F. Romain, A. Neiman, and I. Animitsa, *Solid State Ionics* **145**, 339 (2001).
- [86] B. Huang, J. Schliesser, R. E. Olsen, S. J. Smith, and B. F. Woodfield, *Current Inorganic Chemistry* **4**, 40 (2014).
- [87] Q. Shi, J. Boerio-Goates, and B. F. Woodfield, *The Journal of Chemical Thermodynamics* **43**, 1263 (2011).
- [88] R. Stevens and J. Boerio-Goates, *The Journal of Chemical Thermodynamics* **36**, 857 (2004).
- [89] I. Tanaka, F. Oba, K. Tatsumi, M. Kunisu, M. Nakano, and H. Adachi, *Materials Transactions* **43**, 1426 (2002).



**Table I.** Linear terms from fits to the low temperature ( $T < 15$  K) heat capacity data. Materials in the nanophase are represented by (n). Units of  $\gamma$  are  $\text{mJ}\cdot\text{mol}^{-1}\cdot\text{K}^{-2}$ .

Sample	$\gamma$	Sample	$\gamma$	Sample	$\gamma$
CuO [18]	0.022	$\gamma$ -Al <sub>2</sub> O <sub>3</sub> (n) [41]	1.3542	Sr <sub>2</sub> TiSi <sub>2</sub> O <sub>8</sub> [40]	0.0803
CuO (n)*	0.489	$\gamma$ -Al <sub>2</sub> O <sub>3</sub> (n) [41]	1.3905	BaCuO <sub>2</sub> [23]	10.6
ZnO (n) [38]	0.103	$\gamma$ -Al <sub>2</sub> O <sub>3</sub> (n) [41]	1.22	BaCuO <sub>2</sub> [23]	12.4
Co/ZnO [38]	31.64	$\gamma$ -Al <sub>2</sub> O <sub>3</sub> (n) [41]	1.3912	BaCuO <sub>2.14</sub> [23]	5.7
Co/ZnO (n) [38]	21.635	SnO <sub>2</sub> [37]	0.172	Li <sub>1.2</sub> Ti <sub>1.8</sub> O <sub>4</sub> [16]	3.6
GeCo <sub>2</sub> O <sub>4</sub> [21]	0.33	SnO <sub>2</sub> (n) [37]	0.401	Na <sub>0.25</sub> V <sub>2</sub> O <sub>5</sub> [24]	11.3
CoO [20]	0.4	HfO <sub>2</sub> [39]	0.0793	Na <sub>0.28</sub> V <sub>2</sub> O <sub>5</sub> [24]	9.42
CoO [38]	0.1856	$\gamma$ -FeOOH [27]	0.0927	Na <sub>0.33</sub> V <sub>2</sub> O <sub>5</sub> [24]	9.85
CoO (n) [20]	6.0	$\gamma$ -FeOOH [27]	0.3526	Na <sub>0.40</sub> V <sub>2</sub> O <sub>5</sub> [24]	5.73
Co <sub>3</sub> O <sub>4</sub> *	2.138	$\beta$ -FeOOH [27]	0.1449	K <sub>0.20</sub> V <sub>2</sub> O <sub>5</sub> [24]	15.2
Co <sub>3</sub> O <sub>4</sub> (n)*	8.46	2-line FeOOH [32]	0.1551	Cu <sub>0.40</sub> V <sub>2</sub> O <sub>5</sub> [24]	60.1
Co <sub>3</sub> O <sub>4</sub> (n)*	14.111	$\alpha$ -FeOOH [26]	0.23	Cu <sub>0.55</sub> V <sub>2</sub> O <sub>5</sub> [24]	32.5
TiO <sub>2</sub> rut [22]	0.0993	$\alpha$ -Fe <sub>2</sub> O <sub>3</sub> [33]	0.0362	Cu <sub>0.60</sub> V <sub>2</sub> O <sub>5</sub> [24]	26.4
TiO <sub>2</sub> ana [22]	0.1099	$\alpha$ -Fe <sub>2</sub> O <sub>3</sub> [33]	0.0224	Ag <sub>0.33</sub> V <sub>2</sub> O <sub>5</sub> [24]	8.05
TiO <sub>2</sub> rut (n) [29]	0.508	$\alpha$ -Fe <sub>2</sub> O <sub>3</sub> (n) [31]	1.0235	La <sub>1.98</sub> Ba <sub>0.02</sub> CuO <sub>4</sub> [17]	0.5
TiO <sub>2</sub> rut (n) [29]	0.564	Fe <sub>3</sub> O <sub>4</sub> (n) [19]	3.4619	La <sub>0.7</sub> Ca <sub>0.3</sub> MnO <sub>3</sub> [25]	5.2
TiO <sub>2</sub> rut (n) [29]	0.4994	FePO <sub>4</sub> [36]	13.211	La <sub>0.7</sub> Ba <sub>0.3</sub> MnO <sub>3</sub> [25]	6.1
TiO <sub>2</sub> ana (n) [30]	0.5941	Fe <sub>3</sub> PO <sub>7</sub> [35]	16.32	La <sub>0.7</sub> Sr <sub>0.3</sub> MnO <sub>3</sub> [25]	6.0
TiO <sub>2</sub> ana (n) [30]	0.6564	Fe <sub>3</sub> (P <sub>2</sub> O <sub>7</sub> ) <sub>2</sub> [36]	26.613	Y <sub>0.7</sub> Sr <sub>0.3</sub> MnO <sub>3</sub> [25]	8.1
TiO <sub>2</sub> ana (n) [30]	0.6877	Fe <sub>4</sub> (P <sub>2</sub> O <sub>7</sub> ) <sub>3</sub> [35]	73.69	$\alpha$ -D-xylose [43]	0.4902
Ti <sub>0.78</sub> Al <sub>0.22</sub> O <sub>2</sub> (n) [42]	0.8118	Fe <sub>2</sub> P <sub>2</sub> O <sub>7</sub> [34]	83.61	Muskovite [5]	25.5
Ti <sub>0.5</sub> Al <sub>0.5</sub> O <sub>2</sub> (n) [42]	1.101	SiO <sub>2</sub> [28]	0.066		

\*linear terms and data to be published elsewhere.

**Table II.** Measured lattice vacancy concentrations for several materials. Values of  $n_{vac}$  have been converted into moles of vacancy per mole of formula unit.

<b>Sample</b>	<b><math>n_{vac}</math></b>	<b>Sample</b>	<b><math>n_{vac}</math></b>
C doped TiO <sub>2</sub> [65]	$1.12 \times 10^{-3}$	CeO <sub>2</sub> (5 nm) [60]	$6.01 \times 10^{-3}$
C doped TiO <sub>2</sub> [65]	0.0176	CeO <sub>2</sub> (10 nm) [60]	$2.4 \times 10^{-3}$
TiO <sub>2</sub> as prepared [65]	$9.41 \times 10^{-4}$	CeO <sub>2</sub> (10 nm) [66]	$2.0 \times 10^{-3}$
TiO <sub>2</sub> oxidized [65]	$2.01 \times 10^{-5}$	CeO <sub>2</sub> (15 nm) [68]	$2.4 \times 10^{-4}$
Fe doped TiO <sub>2</sub> [61]	$6.27 \times 10^{-3}$	CeO <sub>2</sub> (20 nm) [60]	$1.2 \times 10^{-4}$
Cr doped SrTiO <sub>3</sub> [67]	$6.6 \times 10^{-4}$	CeO <sub>2</sub> (30 nm) [60]	$2.4 \times 10^{-5}$
LaSrCoO <sub>x</sub> [64]	0.25	CeO <sub>2</sub> (65 nm) [60]	$1.2 \times 10^{-5}$
Sr <sub>2</sub> MgMoO <sub>(6-δ)</sub> [58]	0.05	Fe <sub>3</sub> O <sub>4</sub> [73]	$4.9 \times 10^{-3}$
Ba <sub>0.5</sub> Sr <sub>0.5</sub> Co <sub>0.8</sub> Fe <sub>0.2</sub> O <sub>(3-δ)</sub> [59]	0.661	Fe <sub>3</sub> O <sub>4</sub> (10 nm) [70]	0.036
Ba <sub>0.5</sub> Sr <sub>0.5</sub> Co <sub>0.8</sub> Fe <sub>0.2</sub> O <sub>(3-δ)</sub> [59]	0.807	Fe <sub>3</sub> O <sub>4</sub> (n)*	0.1250
Ce <sub>0.9</sub> Gd <sub>0.1</sub> O <sub>1.95</sub> [69]	0.13	CuO [71]	$6.2 \times 10^{-4}$
La <sub>0.67</sub> Ca <sub>0.33</sub> MnO <sub>(3-y)</sub> [62]	0.065	CuO [57]	$9.8 \times 10^{-4}$
MgO·3.5Al <sub>2</sub> O <sub>3</sub> [72]	0.072	CuO (n)*	0.0109
Co <sub>3</sub> O <sub>4</sub> *	$9.5 \times 10^{-3}$	Cu <sub>2</sub> O [57]	$7.3 \times 10^{-4}$
Co <sub>3</sub> O <sub>4</sub> (n)*	0.1230	SiO <sub>2</sub> [74]	$\sim 3 \times 10^{-4}$
CoO (n)*	0.1639	Al <sub>2</sub> O <sub>3</sub> (n)*	$4.7 \times 10^{-3}$

\*this study

## Figure Legends

**FIG. 1.** Selected linear terms,  $\gamma$ , from fits to the low temperature ( $T < 15$  K) heat capacity data of insulating materials. Hollow symbols represent the nanophase of the material; solid represents bulk. (color online)

**FIG. 2.** Various possible distributions of energy gaps,  $n_{Sch}(\theta)$ , for the Schottky heat capacity arising from lattice vacancies. a) Gaussian distribution. b) Skewed Gaussian distribution. c) Two Gaussian distributions summed. d) Step distribution. See text for more details.

**FIG. 3.** Heat capacities generated by summing Schottky distributions that have  $n_{Sch}$  and  $\theta$  values corresponding to the distributions: a) Gaussian, b) skewed Gaussian, c) sum of two Gaussians, and d) step (as seen in Fig. 2). Plots are of  $C/T$ ; therefore, a linear heat capacity will be a constant in these plots.

**FIG. 4.**  $\gamma$  vs  $n_{vac}$  of several samples. From left to right:  $\text{Al}_2\text{O}_3$  (n),  $\text{Co}_3\text{O}_4$ ,  $\text{CuO}$  (n),  $\text{Co}_3\text{O}_4$  (n),  $\text{Fe}_3\text{O}_4$  (n), and  $\text{CoO}$  (n). Also shown are the lines derived from the four distributions of Schottky anomalies with the slopes (units of  $\text{mJ}\cdot\text{mol}^{-1}\cdot\text{K}^{-2}$ ) shown in parenthesis in the legend.

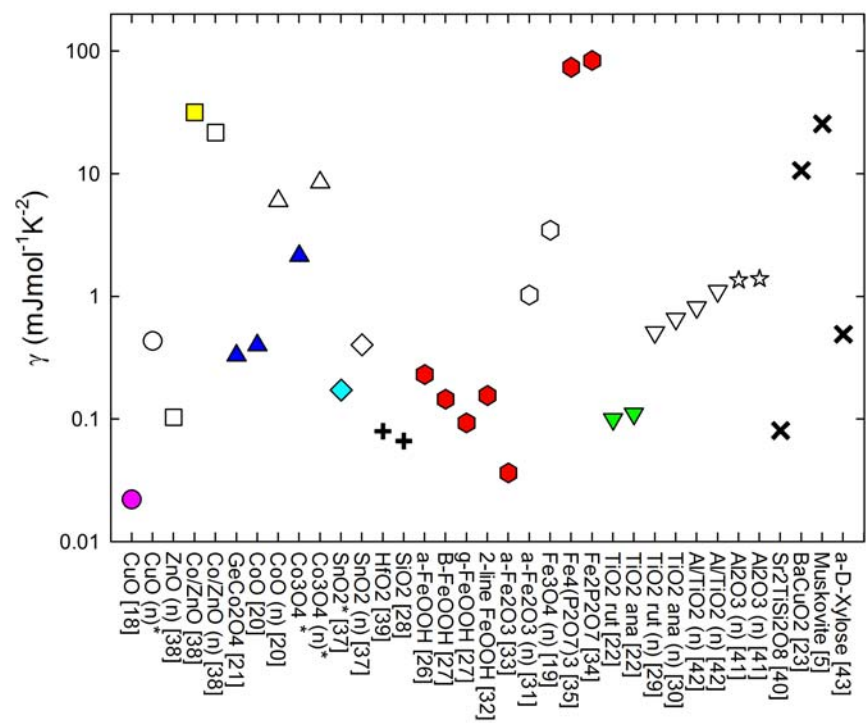
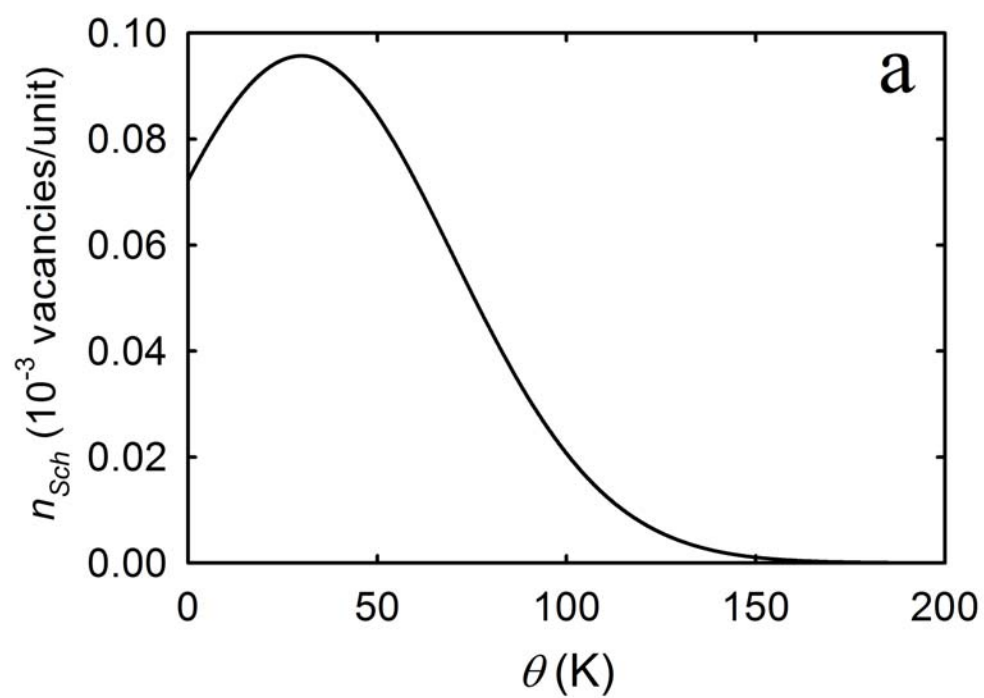
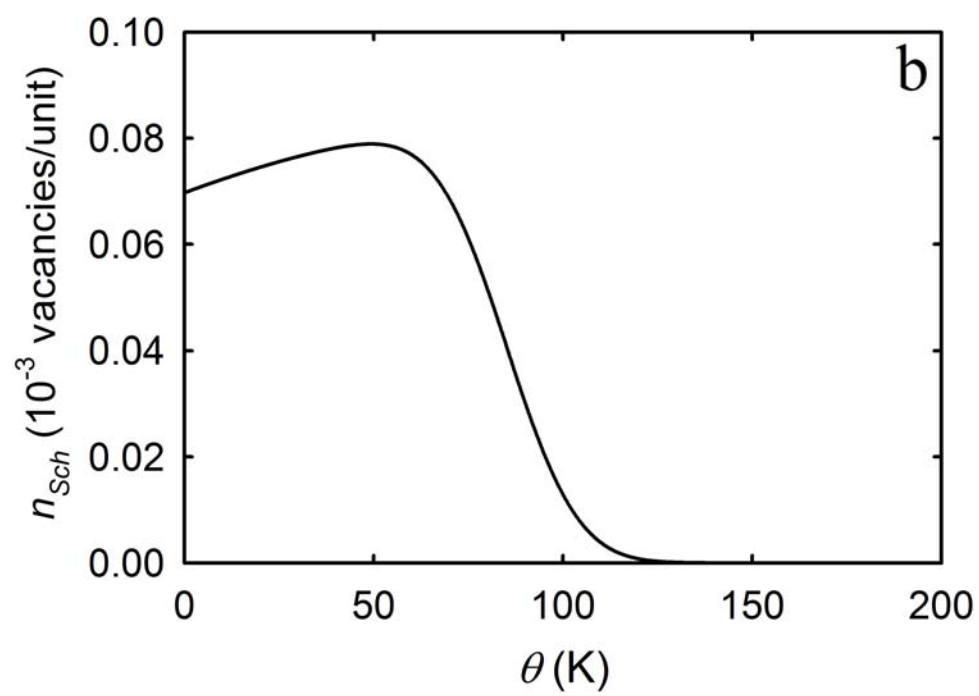


Figure 1.



**Figure 2a.**



**Figure 2b.**

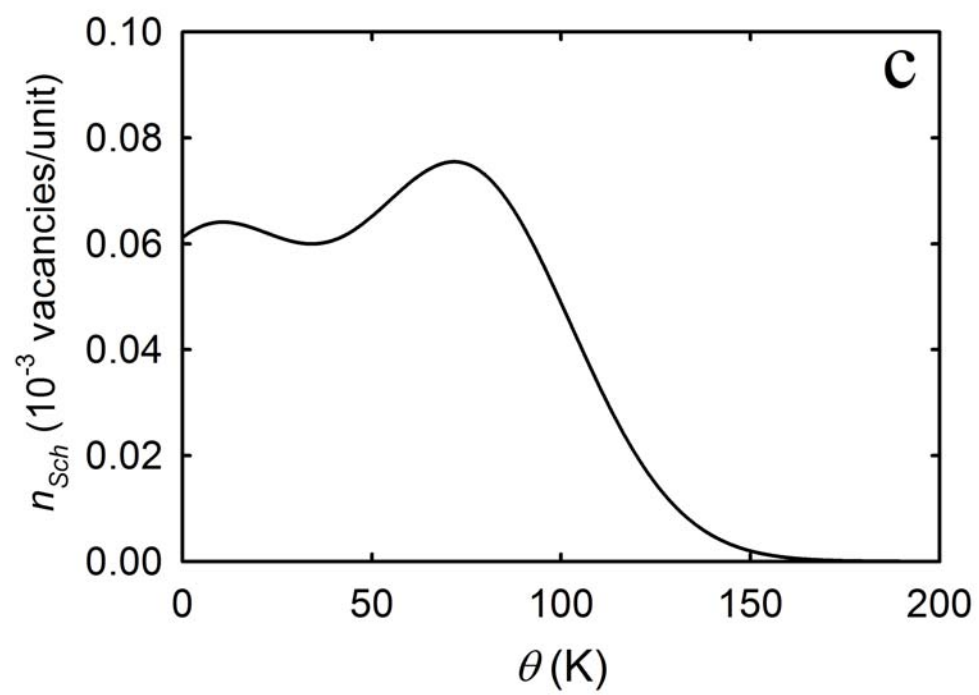


Figure 2c.

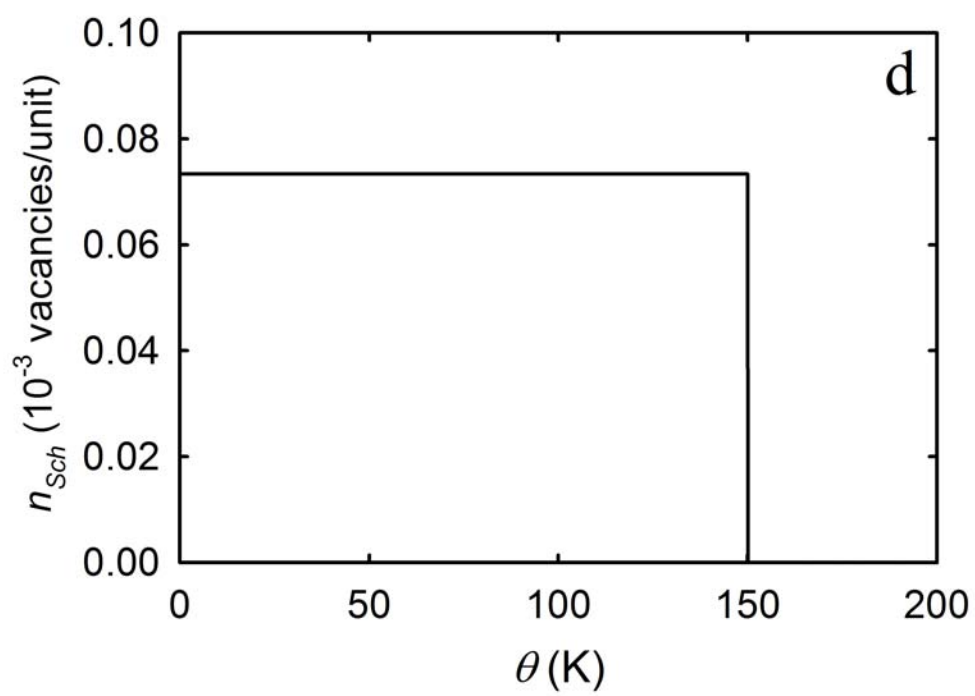
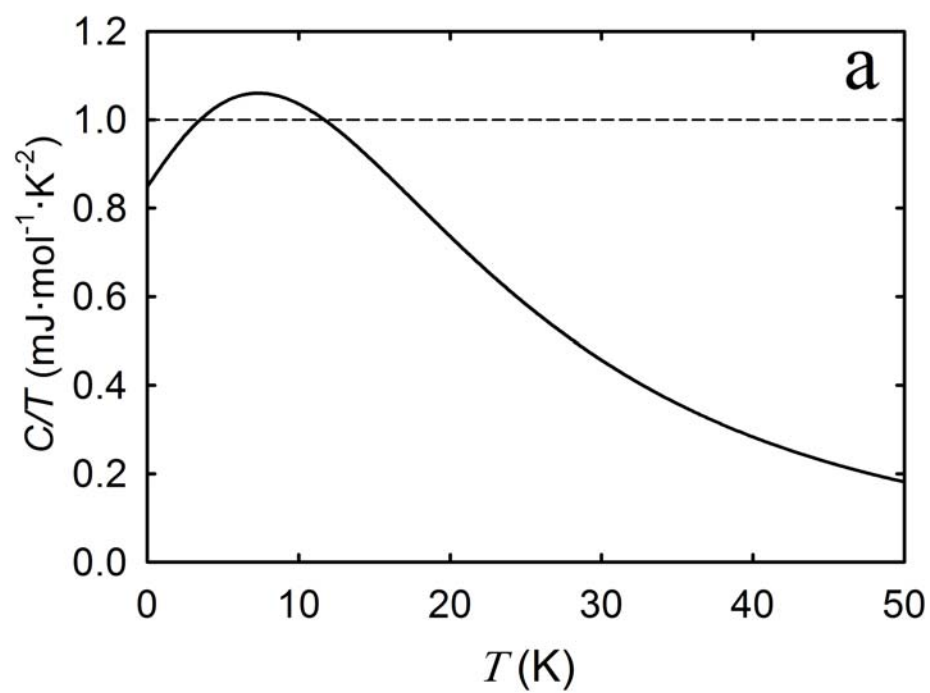
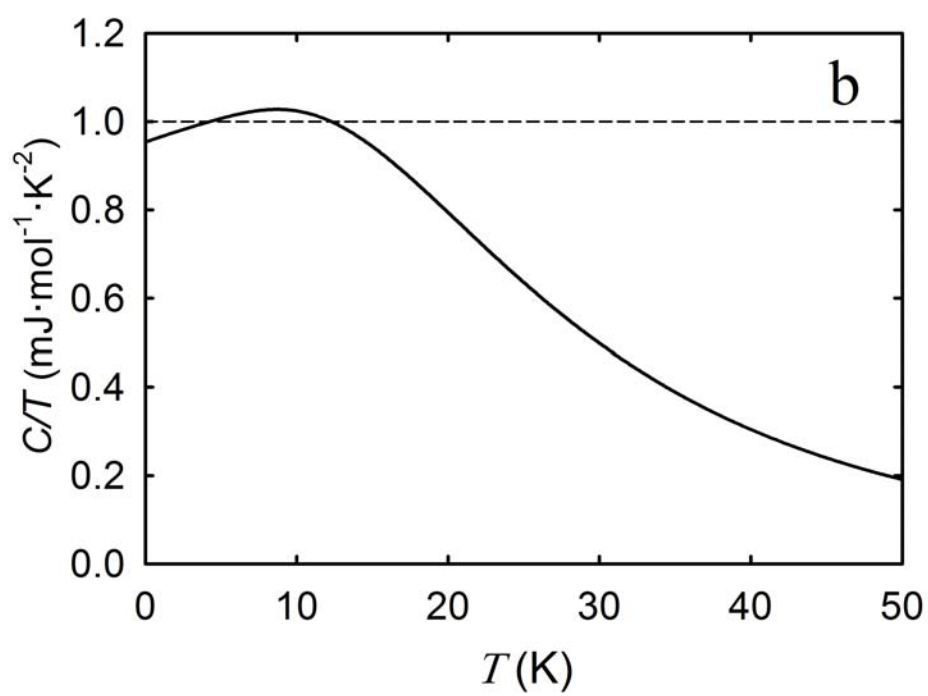


Figure 2d.





**Figure 3a.**



**Figure 3b.**

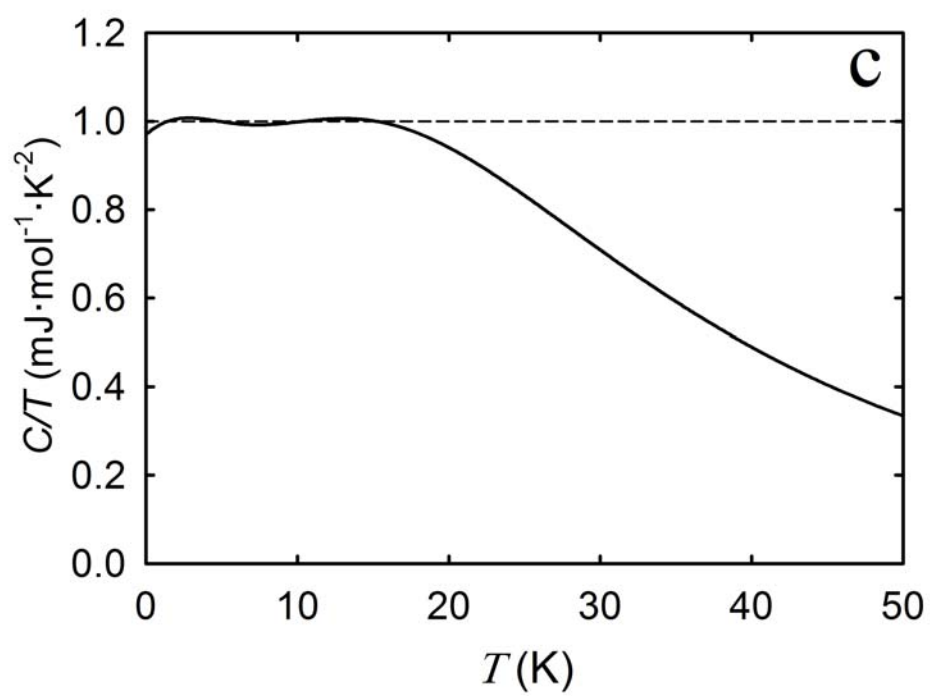


Figure 3c.

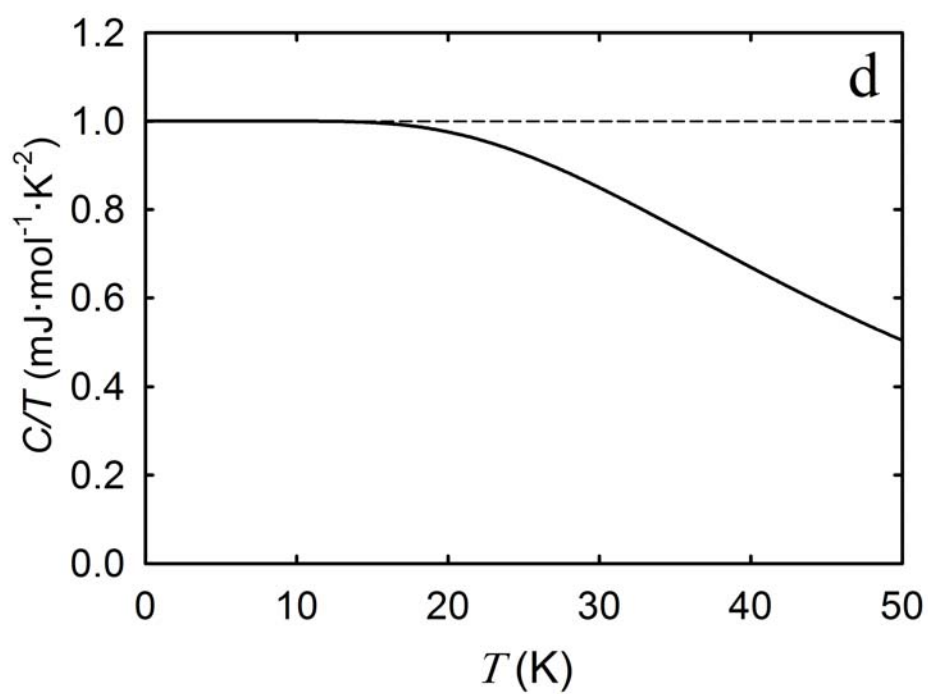
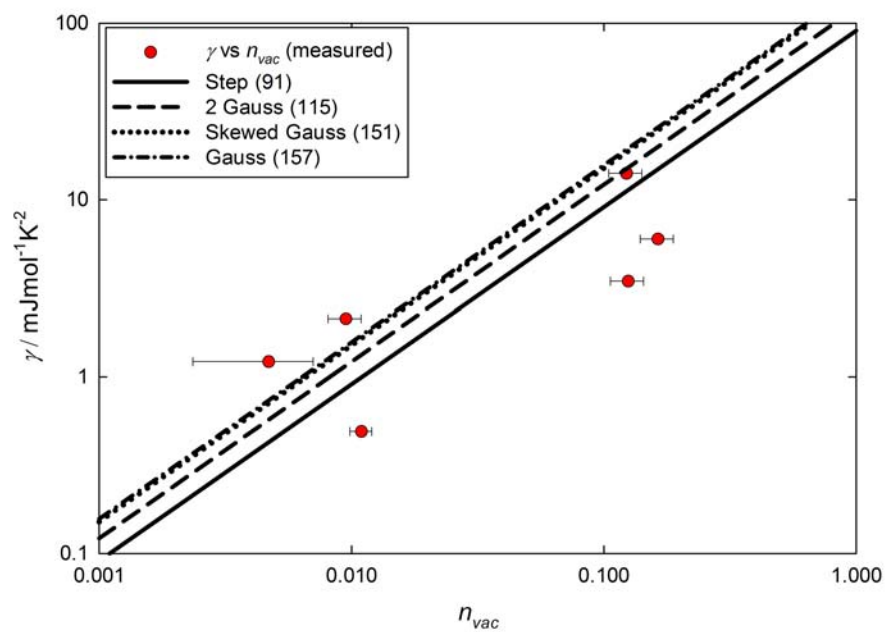


Figure 3d.



**Figure 4.**